

CACTUS as a Reliable Tool for Early Classification of Age-related Macular Degeneration

Luca Gherardini^{a,b,*}, Imre Lengyel^b, Tunde Peto^c, Caroline C.W. Klaver^{d,e,f,g}, Magda A. Meester-Smoor^{d,e}, Johanna Maria Colijn^{d,e}, EYE-RISK Consortium, E3 Consortium, Jose Sousa^{a,c}

^aPersonal Health Data Science Team, Sano Centre for Computational Personalised Medicine, Krakow, Poland

^bThe Wellcome-Wolfson Institute for Experimental Medicine, School of Medicine Dentistry and Biomedical Science, Queen's University Belfast, Belfast, Northern Ireland, the United Kingdom

^cInstitute of Clinical Sciences Building A, Queen's University Belfast, Belfast, Northern Ireland, the United Kingdom

^dDepartment of Epidemiology, Erasmus Medical Center, Rotterdam, the Netherlands

^eDepartment of Ophthalmology, Erasmus Medical Center, Rotterdam, the Netherlands

^fDepartment of Ophthalmology, Radboud University Medical Centre, Nijmegen, the Netherlands

^gInstitute of Molecular and Clinical Ophthalmology Basel, Basel, Switzerland

Abstract

Machine Learning (ML) is widely used to solve various tasks, including disease classification, monitoring, and prediction. The performance of ML models is subject to the availability of significant volumes of complete data. Unfortunately, the data available in real healthcare scenarios is often severely limited or incomplete, impairing the performance of these ML models in practice. While these already limit performance, other problems may also emerge, such as the trustworthiness of solutions depending on the datasets. These limitations, combined with the opacity of some ML models, can make understanding their behaviour and adoption difficult. There is a push for transparent and easily understandable artificial intelligence in several fields, especially healthcare. Age-related Macular Degeneration (AMD) is a retinal disease affecting millions of older adults worldwide. The lack of effective treatments to reverse its progression makes early diagnosis crucial to adopt preventive strategies and identify those at risk of losing sight. Diagnosing AMD mainly relies on assessing retinal images in addition to verbal reports of symptoms by the patients. There is a need for a different classification approach focused on genetic, dietary, clinical, and demographic factors. Recently, we developed a new model called "Comprehensive Abstraction and Classification Tool for Uncovering Structures" (CACTUS) to understand how to classify AMD stages. We propose an application of CACTUS to tackle these issues and provide an explainable and flexible tool for early AMD classification. CACTUS outperforms standard Machine Learning models, helps identify key decision-making factors, and provides confidence in its outcomes to improve decision-making. The features highlighted by CACTUS as the most important for its reasoning allowed us to compare and test them against existing medical knowledge. By removing less relevant or biased information from the dataset, we simulated a clinical scenario involving clinicians who can provide feedback and identify biases.

Keywords: Artificial Intelligence, Age-related Macular Degeneration, Classification, Explainable AI

* Corresponding author Email address: l.gherardini@sanoscience.org (Luca Gherardini)

Introduction

Diagnosing a disease requires dealing with the intrinsic uncertainty of the many parameters available and their interdependence. Artificial Intelligence (AI), and in particular, some of its most relevant sub-categories, such as Machine Learning (ML) and Deep Learning (DL), are widely adopted to address these uncertainties, given that enough data and computational power are provided [1]. However, these requirements are not always feasible. In fields like healthcare, for example, collecting more data might not be possible due to practical reasons (e.g., economic costs, required equipment and staff, and the rarity of a disease) [2]. Another typical property of medical data is the high percentage of missing values and the presence of noise, representing a substantial obstacle for current AI systems [3]. Using DL as a universal learning model is challenging due to its intrinsic lack of transparency, commonly called “black box” [4, 5, 6, 7]. This opacity overshadows its practical effectiveness in modelling and predicting complex patterns, as its internal reasoning is, by default, complex to validate. As such, explaining DL models is challenging, making their adoption in sensitive fields like law, healthcare, and economics debatable [8]. Despite recent efforts to make DL models more explainable [9], it is not easy to overcome their biases and excessive sensitivity towards the input [10]. More explainable models are also easier to *trust* and rely on, which is crucial for integrating AI systems into our society. Imbalances in the dataset can, for example, lead to biases in the classification [3, 9]. The increasing awareness of the role of AI in our daily lives led to regulations to define the liability of an algorithm: the European Union integrated the “right to explainability” in recital 71 of the General Data Protection Regulation (GDPR). At the same time, the US Congress decreed the “Algorithmic Accountability Act” (HR 6580 of 2022) [11, 12]. Interpretable models are essential to understanding decision-making and improving their judgment by detecting malfunctions and biases [13]. Therefore, research is gradually shifting towards increasing the explainability of existing DL models (ad-hoc and post-hoc solutions) or testing altogether different algorithms [6, 14]. Users, such as clinicians and patients, must understand the decisions that AI makes. Evidence suggests that knowledge graphs [15] are particularly suitable for deploying “explainability” and supporting reasoning [16]. They were also used in the biomedical sector to describe concepts, events and their interdependence [17].

Age-related macular degeneration (AMD) is a chronic retinal disease that accounts for 8.7% of world-wide blindness [18]. The number of individuals affected by AMD is expected to increase from 196 million reported in 2020 to 288 million by 2040 [18]. Its development is affected by environmental, dietary, genetic, and lifestyle factors, but data for these factors are often patchy in population-based study datasets. Overall, AMD has two advanced forms: geographic atrophy (GA) and choroidal neovascularisation (CNV); currently, outside of the USA [19], only the latter has available treatment. These are expensive and very demanding for patients, carers, and society due to comorbidities, patient discomfort and, in some cases, diminishing effects or futility [20]. The progression of AMD is slow but irreversible. Therefore, preventive strategies are needed to delay its onset of end-stage disease. Lifestyle and diet changes may reduce the speed and likelihood of progression to later AMD stages [21]. We, therefore,

need to identify and then focus on developing earlier diagnoses to improve the quality of life of people affected by AMD. AMD is usually diagnosed through retinal imaging and image analysis. This diagnosis approach requires trained specialists, specific equipment, and time, and it relies on human interpretation of the images [22]. These elements, combined with increasing demand, are exceeding the capacity of available specialists [22]. Given the limited treatment options and the potential for preventive strategies, early diagnosis is a significant unmet medical need.

The Comprehensive Abstraction and Classification Tool for Uncovering Structures (CACTUS) [23] analyses and *abstracts* data to build knowledge graphs [24], representing potential interaction between different features. CACTUS can handle missing values and noisy data by leveraging novel approaches [23]. To manage the high complexity of AMD classification, CACTUS needed to undergo significant changes and expansion since its last publication to improve its generalisation capabilities and transparency.

Results

CACTUS performance

First, we compared CACTUS against standard ML models for different levels of removed values. For this, we followed our workflow, depicted in Figure 1 and described in the Methods section. To compare these models, we relied on balanced accuracy, which accounts for imbalances between the groups, as described in Table 1. The results, summarised in Table 2, indicate that CACTUS could better differentiate between multiple AMD stages at every level of fragmentation. All algorithms achieved more than the random chance (20% or 1 out of 5) of correctly guessing the right AMD stage. The relationship between the models' balanced accuracy (y-axis) and the percentage of removed values (x-axis) is depicted in Figure 2. The plot shows higher performance of all three CACTUS classification methods (Degree, CDG; Probabilistic, CPB; and PageRank, CPR) compared to traditional ML algorithms: Ridge, Random Forest (RF), Logistic Regression (LR), Stochastic Gradient Descent (SGD), Support Vector Machine (SVM), and eXtreme Gradient Boosting (XGB). PageRank (CPR) showed the highest balanced accuracy in the first three versions of the dataset (0%, 20%, and 40% of missing values), while Degree (CDG) and Probabilistic (CPB) achieved the highest in the 3 most fragmented (40%, 60%, and 80%). The performance degradation due to fragmentation ranged from 4% (CPB) to 8% (Ridge) loss in balanced accuracy from the most complete to the most fragmented dataset in all models.

CACTUS confidence

Figure 3 describes the relationship between the confidence of CPB, CPR, and CDG in assigning AMD stages, their balanced accuracy, and the population. This relationship can set confidence thresholds covering 90%, 80%, 70%, 60%, and 50% of the population, as well as the corresponding classification performance, represented by vertical coloured lines in Figure 3. The more inflated the cumulative lines for confidence and populations, the better the corresponding model. This indicates

that the model performs better while requiring lower confidence. This shows that, despite the good resistance of CPB and CDG to missing values, their confidence and population distributions are skewed to high values (CPB, panels C and D; CDG, panels E and F), meaning that they can be trusted only when they return high confidence levels. Conversely, CPR has a more normally distributed confidence on the population and more inflated cumulative curves (panels A and B), allowing it to provide good coverage of the population with reasonable confidence. For these reasons, we omitted CPB and CDG from further evaluations and discussions, focusing only on CPR. For instance, a confidence threshold of 15% enables us to confidently apply CPR on 50% of the population (brown vertical line), with a balanced accuracy of 27%, which is above the random chance line (20%; orange horizontal line).

CACTUS ranks

After identifying PageRank (CPR) as the most accurate model, we determined the ranks of the nine most influential features in this model (Figure 6). The ranks also describe the distribution of the flips across the classes to show why a feature is important. Flips are values abstracted by CACTUS by finding an optimal threshold to differentiate between AMD stages. Up (U) and Down (D) values represent values above and below this optimal threshold. SNPs, such as ARMS2.rs3750846, have more than two flips representing the three possible alleles. A total list of the ranks returned by CPR, CDG and CPB is available in the supplementary material (Supplementary Table 4). For presentation purposes, the significance of the abstracted values of the same feature was normalised to sum up to 1 in each class. For CPR, the significance of an abstracted value combines its probability of appearing in a given AMD stage with its centrality in the corresponding graph structure. By analysing the clinical features, we found that their significance changes according to the disease stages, while others show a variable dynamic.

Furthermore, we noted that features unrelated to AMD were part of the dataset, for example, those describing the type of tissues collected from the patient. We gave the model feedback and refined the feature pool by excluding those without biological significance for AMD and those with more than 50% missing values. The choice for this threshold reflected the population threshold used to compare CPR, CDG and CPB. After removing these features and rerunning the model, we obtained a new set of ranks, shown in Figure 4, revealing the underlying biology of AMD. Increasing Age (rank 0), mineral and multivitaminic supplements (ranks 1 and 3, respectively), hypercholesterolemia (rank 4), total AMD genetic score (rank 5), and the assumption of anti-trombotic agents (trombo_inh, rank 7), were associated with more advanced disease stages, indicating that older people with a higher genetic predisposition and comorbidities related to AMD are more likely to develop advanced stages. Indeed, this also reveals the obvious information that people with advanced AMD are more inclined to take supplements aimed at slowing its progression. Decreases in best-corrected visual acuity (B_va_dec_os and B_va_dec_od) become a significant determinant at the late stages of the disease. This filtration decreased the balanced accuracy by 0% to 2% for CDG, CPR, and CPB, as shown in Table 3.

Lastly, we ran the model on the nine highest ranks identified in Figure 4 to measure their contribution to the classification task. Table 3 shows that these nine features alone account for most of the model's performance, as the balanced accuracy lost, at most, 5%. Interestingly, CDG achieved a higher accuracy on the 9 highest ranks alone than on the refined dataset, surpassing the other two algorithms.

Discussion

The classification performance of CACTUS highlighted how our algorithm can provide higher balanced accuracy than standard ML models. CACTUS is a useful tool for practical clinical scenarios, as the balanced accuracy quantifies how well an algorithm is expected to perform outside the experimental setting. The random chance to guess the right AMD stage was 20% (1 in 5) in our analysis. Algorithms that perform poorly in controlled testing environments cannot provide reliable performance in real-life applications. The balanced accuracy achieved by each CACTUS method for each version of the dataset is well above this threshold and the other ML methods, showing that the fragmented clinical data used can still provide an informative classification for AMD, and the algorithms were able to extract meaningful patterns to aid a clinician. This was the first time CACTUS was compared with XGBoost, which natively deals with missing values. CACTUS PageRank (CPR) achieved the highest balanced accuracy in 3 out of 5 experiments, as shown in Figure 2, and proved the most solid confidence for applications in real-case scenarios, as displayed in Figure 3. For these reasons, we focused on CPR to analyse its performance in AMD classification. When we refined the dataset to exclude information without biological and clinical relevance for AMD or simply too scarce to be reliable for its classification, we emulated the kind of feedback CACTUS could receive from a clinician in a real-life application. This produced refined ranks (Figure 4) that displayed the interactions inside each AMD stage and how they may change. Therefore, CPR may offer a new perspective on AMD characterisation and classification that outperforms other ML algorithms.

The expansion of CACTUS included a confidence metric for practical clinical scenario approaches, a better abstraction mechanism and graph modelling, and a redesigned classification function. The main advantage of having a measure of confidence is to identify if more data or different expertise is needed to overcome the *knowledge limits*. CACTUS operates based on the available data but can indicate if having more information would make the outcome more reliable. The confidence threshold for accepting the model's decision lacks a formal and objective definition but undoubtedly increases the transparency of the tool and its ease of use. Analogously to probabilities, there is no objective definition of "enough" that can be obtained a priori, but it rather depends on subjective criteria, such as the allowed risk, trust in the system, resources required for collecting more data, and/or availability of other expertise. Despite this lack of an objective way of indicating sufficient confidence, having a measure of it can express how much the model's decision should be trusted. We presented and described the inter-relationship between confidence, balanced accuracy, and population, which allows for customisation of the acceptance criteria of the decision depending on the constraints. This can be used to decide

whether each individual's outcome should be trusted. Furthermore, by combining the confidence with the ranks, the model can signal the most important features that it needs to strengthen its confidence in the output, which would accelerate additional investigations.

Not only did CACTUS prove to have better classification accuracy than traditional ML models, but it also provided insights into its reasoning. Thanks to its transparency, we could compare the elements the algorithm used for the classification. These elements match what is expected from the literature. One of the major factors in AMD is age [25], and CACTUS identified age as the highest rank in determining the stage of the disease. In addition to age, the total genetic score, complement genetic score, and ARSM2 genotype were ranked highly by CACTUS in AMD classification. CACTUS also identified the importance of a slow decline in best-corrected visual acuity as contributing to its prediction. Visual outcomes decline slowly, approximately 1.5 – 2 letters per year in AMD [26]. Some of the features identified as informative on the dataset exhibited an irregular trajectory across the AMD stages. These features were dietary information. These were under-reported in the dataset, showing a noisy and biased distribution. Interestingly, the distributions of these features change the most between stages 3 and 4, probably because dietary interventions are suggested to slow the disease progression, and participants take these as their prognoses worsen [25]. Dietary behaviour can change during the disease progression [27], and, in this case, the proposed approach was able to capture this and exploit it to perform better classification on the few patients who have this information.

We propose CACTUS for diagnosing AMD stages in an explainable way, allowing clinicians to make quicker diagnoses and focus on patients requiring clinical attention, thus optimising scarce resources. Since our goals include reducing the time burden on the clinicians, providing early diagnosis, and allowing for large-scale screenings, we did not train our model on features obtained by medical images; the only exception is the AMD classification that the model aims to predict, which was obtained by grading retinal images. Retinal features are widely analysed and considered in other works on AMD classification and prediction [28, 29, 30, 31, 32, 33, 21, 34, 35]. We still considered general ophthalmic variables, such as visual acuity, as they are easily obtainable without the mentioned constraints. Through the Eye-Risk consortium, we gained access to a dataset on AMD curated by the E3 consortium, on which we applied CACTUS. The Eye-Risk and E3 consortia are two public European research entities specialised in eye diseases, to foster data collection, sharing and collaboration among numerous research groups. This dataset harmonises multiple European studies on AMD, providing a faceted representation of its progression. We found that CACTUS provided representations of each AMD stage and a transparent classification that could be evaluated and tuned against the literature, with high resilience to missing data. Building a holistic representation of the interactions between each pair of elements allows for capturing the complex interdependence AMD relies on. This approach can overcome the challenges of recognising AMD without the information provided by retinal images. We want to exploit the ability of CACTUS to perform classification on smaller and fragmented datasets, combined with a novel notion of confidence, to provide a useful and reliable method for explainable automatic AMD classification.

Using only the available data, CACTUS can be applied more quickly and smoothly in real scenarios, and clinicians can exploit its transparency to validate its reasoning and increase their trust in this tool. This flexibility, uncommon in ML and DL algorithms, can allow for screening large populations, opening new possibilities in healthcare.

Methods

CACTUS provides explainable classifications that are resilient to missing values and noise by applying abstractions. CACTUS ingests data in a tabular format, performs a discretization of its continuous features, and considers the interactions between them to extract meaningful patterns and interactions. We expanded the original tool [23] to better abstract datasets with more than two classes, compute the interactions between highly categorical features more accurately and provide a measure of how confidently each classification was performed. Figure 1 depicts the general steps performed by CACTUS, which will be detailed in the following paragraphs.

Our experiment was conducted on a dataset comprising multiple European studies curated by the EYE-RISK project, through which multidimensional data collection was generated [36]. It gathered genetic, life-related, medical and ophthalmic data from different Europe-wide studies to provide a comprehensive, multifaceted dataset on AMD. We did not input features extracted from retinal images to CACTUS to prove that a meaningful screening approach of AMD is possible. The excluded ophthalmic variables included the presence and size of drusen, Retinal Pigment Epithelium (RPE) detachments, and area and location of dry and wet AMD. The eye with the most advanced AMD determined patients' severity and ranged from 0 (healthy) to 4 (late AMD). Altogether, at most 5 visits per patient were recorded on average every 4 years, covering 25 years. Each visit contains dynamic data such as age, visual acuity at a given visit, blood samples and prescribed drugs. Immutable information, such as genomic data, was recorded only during the first visit and comprised the Single Nucleotide Polymorphisms (SNPs) of 52 common variants associated with AMD. Due to the duration of the study, many patients did not participate in all 5 visits. New patients were enrolled during the considered period, but the turnover was insufficient to replenish the lost participants, leading the later visits to include increasingly fewer people. Furthermore, the proportions between AMD stages are skewed towards healthy individuals for all visits, especially the first. To have both a populous and balanced dataset, we considered the last visit available for each person, obtaining the desired properties. The defined dataset contains 29908 patients and 218 features. The individuals are 55.46% without AMD, 26.85% with stage 1, 10.76% with stage 2, 3.15% with stage 3, and 3.78% with stage 4. A schematic representation of the visits is shown in Table 1.

Abstractions

CACTUS transforms continuous values into discrete elements using an abstraction process. These discrete elements are named *Up* ($_U$) and *Down* ($_D$) *flips*. The abstraction process includes identifying

an optimal *cut-off value* to partition the continuous features. To achieve this transformation, the available classes (i.e., the AMD diagnosis) are temporarily partitioned into two sets, and the values of each feature are considered as a potential discriminator between these two groups. For each feature value, the Receiver Operating Characteristic (ROC) curve is built to consider how well it separates the two sets, and the one returning the highest Balanced Accuracy is used as a cut-off value to transform the continuous values into flips. For instance, 60 years of age may be the most effective cut-off for separating the first class (i.e., no AMD) from the others (i.e., any AMD form); therefore, people with at most 60 years of age will have the flip *Age_D*, and all those who are older will have *Age_U*. Indeed, this approach is straightforward when two classes are available, but it is less straightforward when more are available. The division of the classes into two groups was arbitrary in previous versions of CACTUS. This can be problematic even when there is a plausible differentiation (e.g., no AMD and any form of AMD), as not all features may discriminate between AMD stages in the same way. Some elements could better separate a certain partitioning (e.g., no/early AMD and late AMD) than another one (e.g., no AMD and any AMD), or even just a particular AMD stage (e.g., geographic atrophy) from the rest. For this reason, we present an extension to cover this case, which is an exhaustive search for the best cut-off value over all possible class partitioning and feature values. This guarantees the maximum discriminatory power for each attribute while maintaining the simplicity of having a two-level abstraction. This transformation is applied only to continuous values, which CACTUS recognises automatically by checking if a feature has at most 10 integer values or is specified in its configuration file. Features that are recognised as categorical are just formatted in the same way as the abstracted values (e.g. ARMS2_rs3750846_0, ARMS2_rs3750846_1, and ARMS2_rs3750846_2 represent the three allelic configurations of this SNP).

The Knowledge Graphs

Transforming continuous values into discrete elements allows for computing their probability of being related to each AMD stage and to one another and having a more intuitive representation of reality. CACTUS builds weighted directed graphs using the graph-tool library (<https://graph-tool.skewed.de>) [37]. The connections represent the conditional probability of observing a flip given another. This way, let A_U be the *Up* flip of feature A, and B_U the equivalent flip of feature B, the conditional probability of B_U given A_U in class c is:

$$P(B_U|A_U, c) = \frac{P(A_U \cap B_U|c)}{P(A_U|c)}. \quad (1)$$

This might represent, for instance, the likelihood of having high blood pressure (i.e., *Blood_pressure_U*), being old (i.e., *Age_U*), and having intermediate AMD (i.e., stage 2). The conditional probability is computed only between flips belonging to different features, as flips of the same variables cannot appear together in the same patient (e.g., an individual cannot be simultaneously young and old). As a result, the graph for each class is not fully connected in terms of flips, but it is in terms of features. An improvement over the previous version of CACTUS is how the conditional probabilities are used: rather

than weighing the edges by the conditional probability, their absolute distance from 0.5, which represents independent variables, is used. This way, the connection is weighed by the strength of the influence between the flips. Indeed, this way of connecting flips does not differentiate between positive and negative correlations, but the PageRank and Degree algorithms, explained below, require positive edges to operate correctly.

Graph centrality

Capturing and tracking the interactions of many elements in a disease is fundamental to understanding its causes, origins, and potential treatments. Initially, CACTUS computed the centrality of each component of a particular class exclusively through the PageRank algorithm. This procedure, originally designed and used in Google, ranks web pages using the number and importance of their web links, considering websites referenced by others as more influential. A page referred to by well-linked pages gains a high score itself. PageRank has been used in many scientific disciplines besides web analysis, such as biology and chemistry [38]. One of the vulnerabilities met during CACTUS development [23] was discovered when applying PageRank on graphs with highly categorical features, as the global centrality becomes more homogeneous as the number of connections increases. As a result, these features flatten the centrality, and the network centrality becomes less informative and decisive. The solution we chose was the *total degree* of a flip, which is the sum of the weights of the incoming and outgoing connections. The total degree tracks how well each flip is *locally* interconnected without being reduced by the number of connections in the network, which helped in datasets where categorical features with high (> 10) unique values were stored (data not shown).

After the centrality was computed, the three classification metrics in CACTUS were computed. These are CACTUS Probabilistic (CPB), Degree (CDG), and PageRank (CPR). The first only considers the independent association of each flip to each class, while the other two multiply this metric by the graph centrality they represent. This way, the CPB and the graph centrality-based algorithms, CPR and CDG, model three distinct representations of the flip *significance*.

Classification

Let $\sigma(c, x_i, m)$ be the significance of the flip x_i of the feature x in the class c for the metric m , then the similarity to the class c can be defined as $C_{c,m} = \sum_{i \in N} \sigma(c, x_i, m)$ for all the N features. Therefore, every flip contributes to the cost function of each class with its corresponding significance. The class achieving the highest score is the most similar to the sample and is assigned. In the previous CACTUS publication, the product operation was applied over the flip significances, which represented a vulnerability in situations where flips had centralities close or equivalent to 0, which is very likely in real-case datasets with many missing values. We used CACTUS to build a representation of each AMD stage and assign the most similar one to each individual contained in the dataset. CPB, CPR, and CDG assign different significance scores to the features, providing three distinct classifications.

Interpretation

CACTUS gives the user a detailed representation of the patterns it extracts from the dataset and a measure of confidence in each decision. Confidence and Rank are the two metrics useful in making CACTUS *trustworthy* and *interpretable*.

Rank

The Rank measures how much the significance of the flips of a feature changes between classes, as this difference drives the classification towards the final result. As previously mentioned, the relevance of a flip is obtained by the three classification metrics available in CACTUS: Probabilistic (CPB), PageRank (CPR), and Degree (CDG). First, we compute the Rank R_{m,x_f} of a single flip x_f of a feature x for the metric m as

$$R_{m,x_f} = \frac{\sum_{i=1}^{N-1} \sum_{j>i}^N |\sigma(c_i, m, x_f) - \sigma(c_j, m, x_f)|}{N C_2}, \quad (2)$$

which considers how the significance $\sigma(c_i, m, x_f)$ will change, on average, across the $N C_2$ unsorted pairs of N class instances. The unordered pairs (c_i, c_j) do not assume the classes to be cardinally arranged. Intuitively, the more the significance of x_f changes, the more valuable it will be for classification, as it will provide different contributions to the different classes, lowering or raising the similarity with it. The Rank can then be averaged over the F_x flips of the feature x as

$$\bar{R}_{m,x} = \frac{1}{|F_x|} \sum_{f \in F_x} R_{m,x_f}. \quad (3)$$

The average Rank describes the influence of the feature in differentiating the available classes.

Confidence

Determining the most powerful features in discriminating between the available classes allows for validating the model behaviour and checking for biases and/or erratic reasoning. On the other hand, understanding how *confident* the model is when it assigns a label is a valuable metric to know how much it should be *trusted* when assigning an outcome. We computed the confidence in a patient's outcome as the average absolute difference between the cost of each class i , C_i . This is modelled as

$$\text{Confidence} = \frac{\sum_{i \neq m}^N |C_m - C_i|}{N - 1}, \quad (4)$$

where N is the number of classes, and m is the class that achieved the maximum similarity during classification, formally defined as $m = \text{argmax}(C)$. Intuitively, the model is very confident if only one class has a high significance, while it is more uncertain when all significance scores are close. The confidences are then normalised in the interval $[0, 100]$.

Guidotti et al. [13] defined an important pillar of explainable systems called *knowledge limits*. They indicate cases in which the model was not designed or approved for, or when the model's knowledge is insufficient to answer reliably. Intuitively, when the model indicates low confidence, the user could

provide additional information or rely more on the clinician to obtain a more solid classification. The definition of sufficient confidence evades a strict and universal definition but is somewhat dependent on the application, such as the allowed risk, the cost of gathering more information to increase the confidence of the model or consulting other specialists [39].

Comparison against standard Machine Learning algorithms

To showcase the full potential of CACTUS in differentiating AMD, we chose standard ML models as contenders: Ridge [40], Logistic Regression (LR) [41], Support Vector Machine (SVM) [42], Stochastic Gradient Descent (SGD) [43], Random Forest (RF) [44], and XGBoost (XGB) [45]. All were directly available in the scikit-learn Python library [46, 47], but XGBoost was available through a dedicated Python package. This was the first time we compared CACTUS against XGBoost, which can also natively deal with missing values. The AMD features were scaled using the *StandardScaler* class available before inputting them to ML models, and a 80/20% split for the training/testing phases was applied. A 10-fold Cross-Validation was applied to each model to provide consistent results. For all the considered ML models but XGBoost, the missing values were filled with the average value in the corresponding column; XGBoost did not need this procedure as it automatically learns how to handle missing values [45].

CACTUS makes the most out of small datasets due to its measures against overfitting. As described by Ying [48], overfitting happens due to “the presence of noise, the limited size of the training set, and the complexity of classifiers”. CACTUS reduces the noise contained in the dataset by applying its abstraction mechanism and exploiting a slim set of parameters, corresponding to one weight (significance) per flip for each class, to perform classification. Finally, as described by White [49] and Hellström [50], “in the statistical context there is no such thing as overtraining when there is a weak model that has low complexity and operates on data with low-level noise”. Since CACTUS does not make any assumptions (weak model) on how the real process works, since it builds an almost fully connected graph between flips to describe each class, and considers very few parameters, none of them set *a priori*, after applying abstractions to reduce noise, we can consider CACTUS to mitigate overtraining.

We incrementally and randomly removed values from the EYE-RISK dataset to demonstrate the model’s capability and practical utility in real scenarios, particularly its resilience to missing values. Therefore, CACTUS and the other ML models were tested against the original and fragmented versions of the dataset (20%, 40%, 60%, and 80% of the values were randomly removed). Notably, the original dataset already exhibited missing information. After performing this comparison, we used the confidence metric to determine which of the three classification methods (CPB, CPR, and CDG) was the most reliable in real-case scenarios; this evaluation chose the model with the highest Balanced Accuracies for the 50%, 60%, 70%, 80% and 90% of the population. This criterion is because such a model is more trustworthy, as it will generally perform better for every confidence threshold.

Acknowledgements

We are deeply thankful to the EYE-RISK consortium: Soufiane Ajana¹, Audrey Cougnard-Grégoire¹, Cécile Delcourt¹, Bénédicte M.J. Merle¹, Blanca Arango-Gonzalez², Sascha Dammeier², Sigrid Diether², Sabina Honisch², Ellen Kilger², Verena Arndt³, Tanja Endermann³, Vaibhav Bhatia⁴, Shomi S. Bhattacharya⁴, Sofia M. Calado⁴, Berta De la Cerda⁴, Francisco J. Diaz-Corrales⁴, Marc Biarnés⁵, Anna Borrell⁵, Lucia L. Ferraro⁵, Míriam Garcia⁵, Jordi Monés⁵, Eduardo Rodríguez⁵, Sebastian Bühren⁶, Johanna M. Colijn^{7,8}, Magda Meester-Smoor^{7,8}, Elisabeth M. van Leeuwen^{7,8}, Timo Verzijden^{7,8}, Caroline C.W. Klaver^{7,8,9}, Eiko K. de Jong⁹, Thomas J. Heesterbeek⁹, Carel B. Hoyng⁹, Eveline Kersten⁹, Anneke I. den Hollander^{9,10}, Eszter Emri¹¹, Imre Lengyel¹¹, Hanno Langen¹², Cyrille Maugeais¹², Everson Nogoceke¹², Phil Luthert¹³, Tunde Peto¹⁴, Frances M. Pool¹⁵, Marius Ueffing^{2,16}, Karl U. Ulrich Bartz-Schmidt^{2,16}, and Markus Zumbansen¹⁷. And the European Eye Epidemiology Consortium for granting us access to the data used in this study: Niyazi Acar¹⁶, Eleftherios Anastosopoulos¹⁷, Augusto Azuara-Blanco¹⁸, Arthur Bergen¹⁹, Geir Bertelsen²⁰, Christine Binquet²¹, Alan Bird²², Lionel Brétilon¹⁶, Alain Bron²¹, Gabrielle Buitendijk⁴³, Maria Luz Cachulo²³, Usha Chakravarthy¹⁸, Michelle Chan²⁴, Petrus Chang²⁵, Johanna M. Colijn^{8,7}, Audrey Cougnard-Grégoire²⁶, Catherine Creuzot-Garcher²¹, Philippa Cumberland²⁷, José Cunha-Vaz²³, Vincent Daien²⁸, Gabor Deak²⁹, Cécile Delcourt²⁶, Marie-Noëlle Delyfer²⁶, Anneke den Hollander³⁰, Martha Dietzel³¹, Maja Gran Erke²⁰, Sascha Fauser³², Robert Finger²⁵, Astrid Fletcher³³, Paul Foster²⁴, Panayiota Founti¹⁷, Arno Göbel²⁵, Theo Gorgels¹⁹, Jakob Grauslung³⁴, Franz Grus³⁵, Christopher Hammond³⁶, Catherine Helmer²⁶, Hans-Werner Hense³¹, Manuel Hermann³², René Hoehn³⁵, Ruth Hogg¹⁸, Frank Holz²⁵, Carel Hoyng³⁰, Nomdo Jansonius⁴³, Sarah Janssen¹⁹, Anthony Khawaja²⁴, Caroline Klaver⁴³, Jean-François Korobelnik²⁶, Julia Lamparter³⁵, Mélanie Le Goff²⁶, Sergio Leal²³, Yara Lechanteur³⁰, Terho Lehtimäki³⁷, Andrew Lotery³⁸, Irene Leung²², Matthias Mauschwitz²⁵, Bénédicte Merle²⁶, Verena Meyer zu Westrup³¹, Edoardo Midena³⁹, Stefania Miotto³⁹, Alireza Mishahi³⁵, Sadek Mohan-Saïd⁴⁰, Alyson Muldrew¹⁸, Michael Mueller³⁷, Sandrina Nunes²³, Konrad Oexle⁴¹, Tunde Peto²², Stefano Piermarocchi³⁹, Elena Prokofyeva²⁸, Jugnoo Rahi²⁴, Olli Raitakari³⁷, Luisa Ribeiro²³, Maria-Bénédicte Rougier²⁶, José Sahel⁴⁰, Aggeliki Salonikiou¹⁷, Clarisa Sanchez³⁰, Steffen Schmitz-Valckenberg²⁵, Cédric Schweitzer²⁶, Tatiana Segato³⁹, Jasmin Shehata²⁹, Rufino Silva²³, Giuliana Silvestri¹⁸, Christian Simader²⁹, Eric Souied⁴², Henriët Springelkamp⁴³, Robyn Tapp³⁷, Fotis Topouzis¹⁷, Virginie Verhoeven⁴³, Therese Von Hanno²⁰, Stela Vujosevic³⁹, Katie Williams³⁶, Christian

Wolfram³⁵, Jennifer Yip²⁴, Jennyfer Zerbib⁴², and Isabella Zwiener³⁵.

1. University Bordeaux, Inserm, Bordeaux Population Health Research Center, Team LEHA, UMR 1219, Bordeaux, France.
2. Centre for Ophthalmology, Institute for Ophthalmic Research, Eberhard Karls University Tübingen, University Clinic Tübingen, Tübingen, Germany.
3. Assay Development, AYOXXA Biosystems GmbH, Cologne, Germany.
4. Department of Regeneration and Cell Therapy, Andalusian Molecular Biology and Regenerative Medicine Centre (CABIMER), Seville, Spain.
5. Barcelona Macula Foundation, Barcelona, Spain.
6. Business Development, AYOXXA Biosystems GmbH, Cologne, Germany.
7. Department of Epidemiology, Erasmus Medical Center, Rotterdam, Netherlands.
8. Department of Ophthalmology, Erasmus Medical Center, Rotterdam, Netherlands.
9. Department of Ophthalmology, Radboud University Medical Center, Nijmegen, Netherlands.
10. Department of Human Genetics, Radboud University Medical Center, Nijmegen, Netherlands.
11. Centre for Experimental Medicine, Queen's University Belfast, Belfast, United Kingdom.
12. Roche Innovation Center Basel, F. Hoffmann-La Roche Ltd, Basel, Switzerland.
13. Institute of Ophthalmology, University College London, London, United Kingdom.
14. Centre for Public Health, Queen's University Belfast, Belfast, United Kingdom.
15. Ocular Biology, UCL Institute of Ophthalmology, London, United Kingdom.
16. Inra-University of Burgundy, Dijon, France.
17. University of Thessaloniki, Thessaloniki, Greece.
18. Queen's University Belfast, Belfast, the UK.
19. Netherlands Institute for Neurosciences-KNAW, Amsterdam, the Netherlands.
20. University of Tromsø, Tromsø, Norway.
21. University Hospital of Dijon, Dijon, France.
22. Moorfield's Eye Hospital, London, the UK.
23. AIBILI/CHUC, Coimbra, Portugal.
24. UCL Institute of Ophthalmology, London, the UK.
25. University of Bonn, Bonn, Germany.
26. University of Bordeaux Segalen, Bordeaux, France.
27. UCL Institute of Child Health, London, the UK.
28. Inserm U1061, Montpellier, France.
29. Medical University of Vienna, Vienna, Austria.
30. Radboud University, Nijmegen, the Netherlands.
31. University of Muenster, Muenster, Germany.
32. University Eye Hospital, Cologne, Germany.
33. London School of Hygiene and Tropical Medicine, London, the UK.
34. University of Southern Denmark, Odense, Denmark.
35. University Medical Center Mainz, Mainz, Germany.
36. King's College, London, the UK.
37. Pirkanmaa Hospital District, Tampere, Finland.
38. University of Southampton, Southampton, the UK.
39. University of Padova, Padova, Italy.
40. Institut de la Vision, Paris, France.
41. Institute of Human Genetics, Munich, Germany.
42. University Hospital of Créteil, Créteil, France.
43. Erasmus Medical Center, Rotterdam, the Netherlands.

This publication is supported by two projects funded by the European Union's Horizon 2020 Research and Innovation Programme: the EYE-RISK project - grant agreement No 634479, and the Sano project - grant agreement No 857533. The Sano Project has also received funding from the International Research Agendas Programme of the Foundation for Polish Science - No MAB PLUS/2019/13, and the Minister of Science and Higher Education "Support for the activity of Centres of Excellence established in Poland under Horizon 2020" based on the contract number MEiN/2023/DIR/3796. Luca Gherardini has been employed at the Sano Centre for Computational Medicine and supported by the Queen's University Belfast Postgraduate Support. The Kelvin-2 research cluster of the NI-HPC centre at Queen's University Belfast supported this research.

The authors are deeply grateful to Professor Roger Woods and Varun Ravi Varma, who provided invaluable suggestions for improving the quality of this manuscript.

Authors' contributions

Conceptualisation: LG, IL, JS. Data curation: IL, TP, CCWK, MAMS, JMC. Formal analysis: LG, IL, TP. Investigation: LG, IL. Methodology: LG, JS. Software: LG. Supervision: JS, IL, TP. Validation: JS, IL, TP. Visualisation: LG. Writing - original draft: LG, IL, TP. Writing - review and editing: LG, IL, TP, CCWK, MAMS, JMC, JS.

Declaration of interests

The authors do not have any conflicting interests to declare.

Ethics statement

This study complied with relevant laws and institutional guidelines. The data processed in this study were collected before this work. Therefore, no ethical approval was required. The personal information of each individual was anonymised.

Figures, figure titles, and figure legends

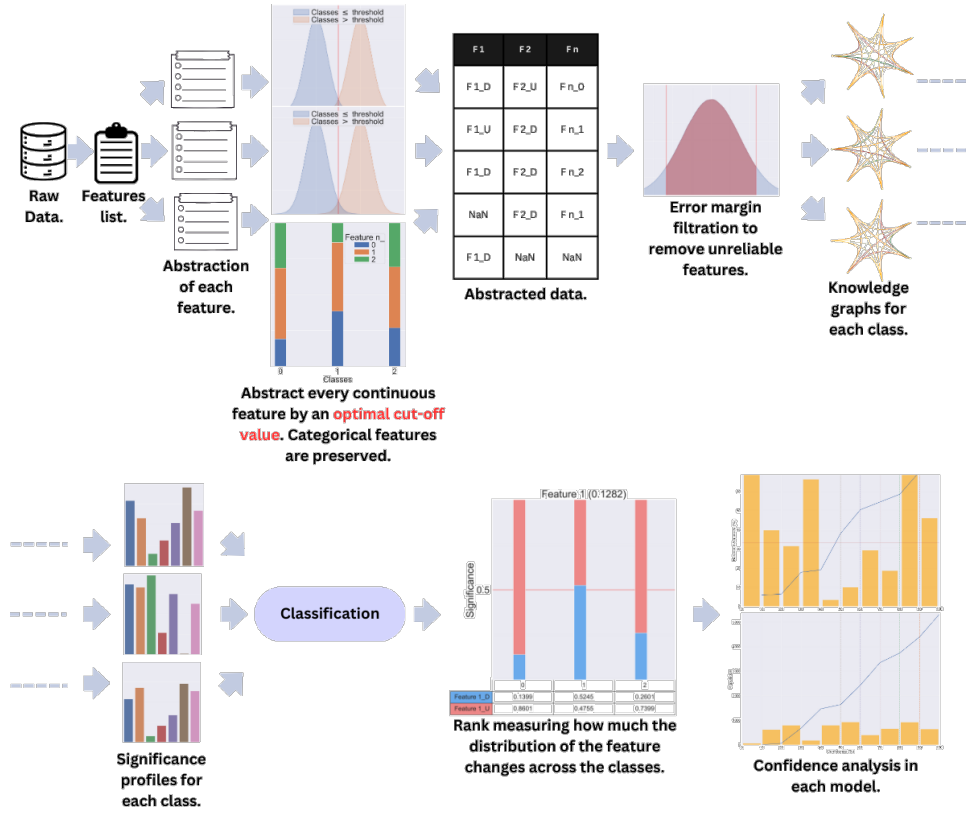


Figure 1: **A diagram of the internal functioning of CACTUS.** Each continuous feature in the dataset is partitioned into *flips* representing high (.U) or low (.D). Otherwise, it is kept unaltered. The threshold to partition the continuous features is found using a receiver operating characteristic (ROC) curve. Two populations are required to build the ROC curve and find the most appropriate threshold to abstract the features. These are created by partitioning the available AMD classes (e.g., by considering the healthy individuals as one population and all the AMD groups as another) into two groups. In previous versions, the user had to select a universal threshold to divide the classes, which required prior domain knowledge and multiple comparisons. Still, CACTUS has since been improved to select the most appropriate threshold for each feature, which is a more sensitive approach to consider the uniqueness of each feature in distinguishing between a certain set of classes. Discrete values allow for building a knowledge graph representing each class by linking the elements by their conditional probability. The centralities computed on these represent a Significance profile. Thus, the classification process compares each individual against the available representations to assign the most similar one. The classification is then applied to all the available individuals to assess the performance. The significance of each flip in each class is analysed to identify the elements driving the classification and provide an explanation for the behaviour of the model.

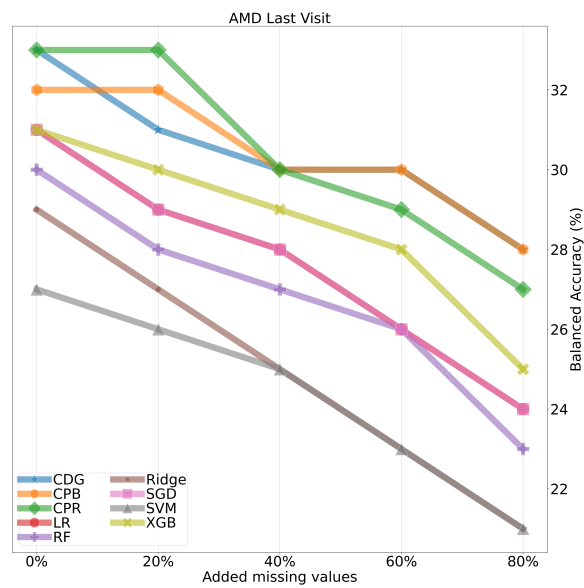


Figure 2: **The performance achieved by CACTUS compared with ML models.** CACTUS's Degree (CDG, blue stars), PageRank (CPR, green diamonds), and Probabilistic (CPB, orange hexagons) implementations are shown along standard ML models: Linear Regression (LR, red circles), Random Forest (RF, purple plus signs), Ridge (brown dots), Stochastic Gradient Descent (SGD, pink squares), Support Vector Machine (SVM, grey triangles), and eXtreme Gradient Boosting (XGB, yellow Xs). X-axis: the percentage of values that were removed from the dataset. Y-axis: the balanced accuracy achieved by the algorithms in distinguishing between AMD stages. 20% represents the random chance of correctly guessing the right AMD stage.

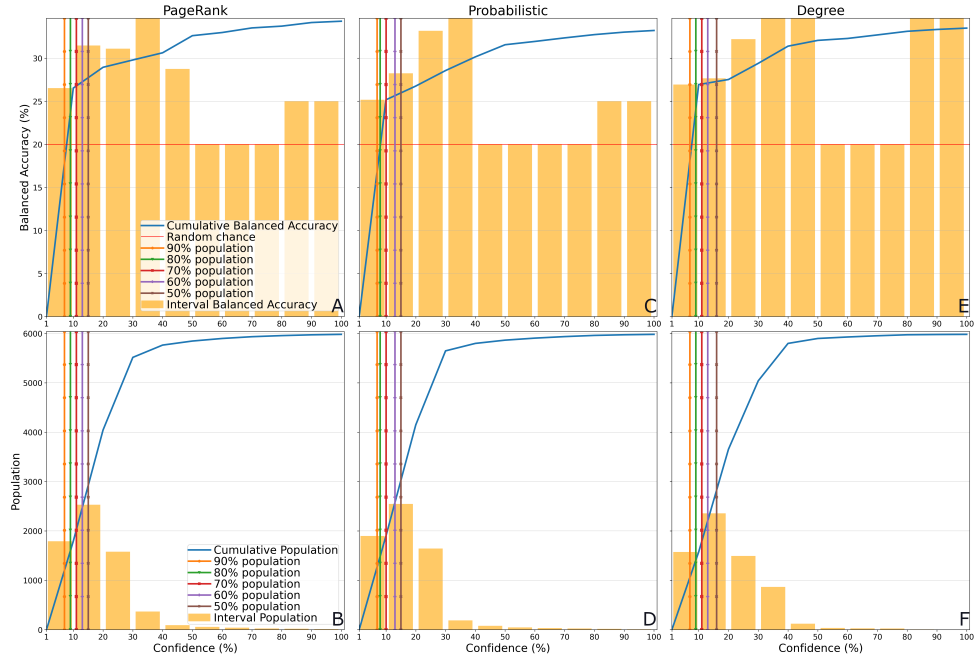


Figure 3: **The relationship between confidence (X-axis), balanced accuracy (Y-axis, first row), and population (Y-axis, second row).** Confidence is reported on the X-axis, while balanced accuracy and population are reported on the Y-axis of, respectively, the first and second rows. This metric is provided for the Degree (A, B), PageRank (C, D), and Probabilistic (E, F) classification methods in CACTUS. The confidence (blue line) is computed as the similarity of a sample to the most similar class compared to its closeness to the others. The yellow bins (bars) represent the values (the balanced accuracy in panels A, C, and E; the number of people in panels B, D, F) corresponding to a confidence interval (e.g., the performance of CPR when it has a confidence between 20% and 30%). The population is expressed as the number of people for which a given algorithm had a certain confidence level. Cumulative values (blue lines) represent the balanced accuracy/population when incrementally including all the intervals (yellow bins) on their left side (e.g., the cumulative balanced accuracy at 20% is the average of the balanced accuracy in the $[0, 10)$, $[10, 20]$ bins). The cumulative balanced accuracy is weighted by the number of people in the corresponding bins in the lower plots). The vertical lines represent the confidence levels to cover 90%, 80%, 70%, 60%, and 50% of the population. The horizontal orange line crossing panels A, C, and E represents the random balanced accuracy, which can be used as another indicator for comparing the quality of the models.

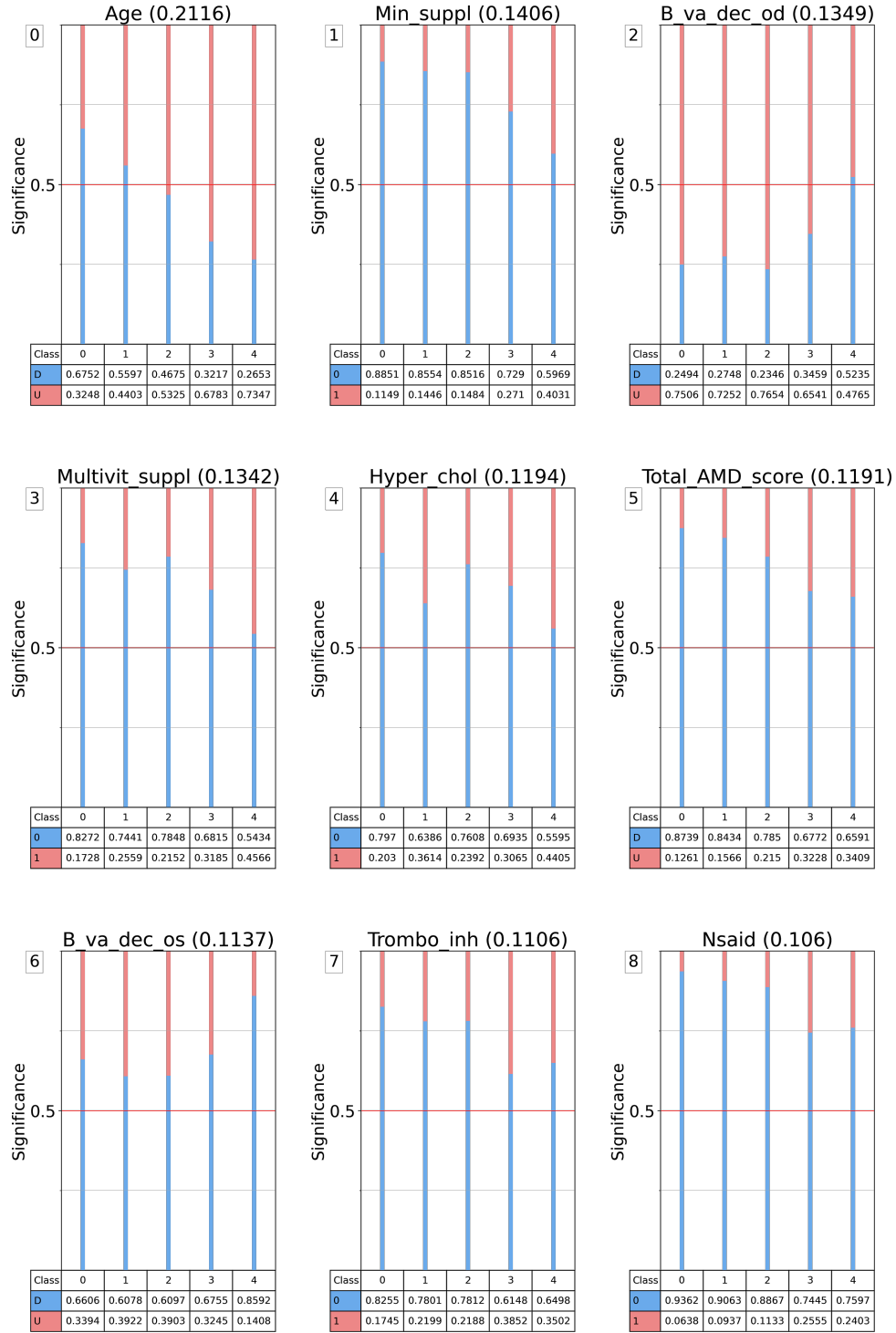


Figure 4: **The ranks of the 9 most important features for the PageRank metric computed on the filtered dataset.** The most relevant features are sorted from the highest (upper left, 0) to the lowest (lower right, 8), as indicated in the title of each plot between parentheses. The distribution of each abstracted value (Down in blue and Up in pink) for each AMD stage (0, 1, 2, 3, 4) is shown. Up (U) and Down (D) represent values above and below the optimal threshold found by CACTUS during the abstraction process.

Tables, table titles, and table legends

		Visit						
		1	2	3	4	5	First	Last
AMD Stage	0	18168 (62.84%)	6590 (55.25%)	2588 (40.52%)	1239 (39.62%)	528 (34.33%)	18624 (62.27%)	16588 (55.46%)
	1	6790 (23.49%)	3911 (32.79%)	2599 (40.69%)	1290 (41.25%)	580 (37.71%)	7161 (23.94%)	8029 (26.85%)
	2	2497 (8.64%)	1012 (8.48%)	696 (10.9%)	377 (12.06%)	255 (16.58%)	2616 (8.75%)	3219 (10.76%)
	3	636 (2.2%)	224 (1.88%)	216 (3.38%)	112 (3.58%)	116 (7.54%)	657 (2.2%)	942 (3.15%)
	4	819 (2.83%)	190 (1.59%)	288 (4.51%)	109 (3.49%)	59 (3.84%)	850 (2.84%)	1130 (3.78%)
Total		28910	11927	6387	3127	1538	29908	29908
Dropped			17526	6775	3560	1695		
New			543	1235	300	106		
Average age per stage	0	66.76	66.23	71.65	74.24	78.3	66.87	69.56
	1	69.61	68.94	72.77	74.51	78.31	69.83	73.0
	2	72.6	71.86	75.21	76.46	79.86	72.75	74.6
	3	74.56	74.72	76.83	78.97	80.34	74.56	76.78
	4	76.32	80.06	79.3	81.24	83.53	76.61	78.44

Table 1: **Description of each visit in the EYE-RISK dataset.** Additional groups comprising, respectively, the first and last visit of each patient have been considered. For each group, the number and percentage of people affected by a particular AMD stage have been reported, in addition to the number of dropped and newly enrolled patients. The average age (in years) was reported during each visit. It is noticeable how healthy patients (first row) are the most prevalent stage recorded before declining towards the end of the study. While this ensures a more balanced dataset, the total amount of patients is also dramatically decreasing due to heavy dropouts. Considering the First and, in particular, the Last visit for each patient, we can obtain sensibly larger cohorts and more balanced proportions. Due to the better balance of the Last visit, we selected this group for further analysis.

Missing values added to Last Visit	CDG	CPB	CPR	LR	RF	Ridge	SGD	SVM	XGB
0%	0.33±0.01	0.32±0.01	0.34±0.01	0.31±0.01	0.3±0.01	0.29±0.01	0.31±0.01	0.27±0.0	0.31±0.01
20%	0.31±0.01	0.32±0.02	0.33±0.01	0.29±0.01	0.28±0.0	0.27±0.0	0.29±0.01	0.26±0.0	0.3±0.01
40%	0.3±0.01	0.3±0.01	0.3±0.01	0.28±0.01	0.27±0.0	0.25±0.01	0.28±0.01	0.25±0.0	0.29±0.0
60%	0.3±0.02	0.3±0.02	0.29±0.02	0.26±0.0	0.26±0.0	0.23±0.0	0.26±0.01	0.23±0.01	0.28±0.0
80%	0.28±0.01	0.28±0.01	0.27±0.01	0.24±0.0	0.23±0.0	0.21±0.0	0.24±0.01	0.21±0.0	0.25±0.0

Table 2: **The balanced accuracy, in percentage, achieved by CACTUS's modalities *Degree* (CDG), *Probabilistic* (CPB), and *PageRank* (CPR) in comparison to standard ML techniques.** In addition to the original dataset of the last visits, we extended the analysis to different percentages of induced missing values to test the model's resilience. All CACTUS modalities performed better than ML models for all datasets, with PageRank achieving the highest performance in 3 out of 5 experiments. All models have been tested through a 10-fold cross-validation approach and an 80/20 split for train/test sets. The standard deviation across the cross-validation was included along the average balanced accuracy.

	BA on the whole dataset (%)	BA on the refined dataset (%)	BA on the 9 highest ranks (%)
CDG	33±0.01	26±0.00	31±0.01
CPB	32±0.01	33±0.01	29±0.01
CPR	34±0.01	34±0.01	29±0.01

Table 3: **The Balanced Accuracy (BA) achieved by the three classification metrics in CACTUS for the whole dataset, a refined set of features, and a selection of the 9 most important features.** The dataset was refined by excluding features without biological significance for AMD or with more than 50% missing values. The 9 features with the highest rank in this refined version are shown in Figure 4. The features in these three sets were 173, 112, and 9.

References

- [1] A. Adadi, A survey on data-efficient algorithms in big data era, Vol. 8, Springer International Publishing, 2021. doi:10.1186/s40537-021-00419-9.
URL <https://doi.org/10.1186/s40537-021-00419-9>
- [2] J. Lee, C. Liu, J. Kim, Z. Chen, Y. Sun, J. R. Rogers, W. K. Chung, C. Weng, Deep learning for rare disease: A scoping review, *Journal of Biomedical Informatics* 135 (2022) 104227. doi:<https://doi.org/10.1016/j.jbi.2022.104227>.
URL <https://www.sciencedirect.com/science/article/pii/S1532046422002325>
- [3] F. Wang, A. Preininger, AI in Health: State of the Art, Challenges, and Future Directions, *Yearbook of medical informatics* 28 (1) (2019) 16–26. doi:10.1055/s-0039-1677908.
- [4] G. S. Handelman, H. K. Kok, R. V. Chandra, A. H. Razavi, S. Huang, M. Brooks, M. J. Lee, H. Asadi, Peering Into the Black Box of Artificial Intelligence: Evaluation Metrics of Machine Learning Methods, *American Journal of Roentgenology* 212 (1) (2019) 38–43. doi:10.2214/AJR.18.20224.
URL <http://services.igi-global.com/resolvedoi/resolve.aspx?doi=10.4018/978-1-59904-949-6.ch067><https://www.ajronline.org/doi/10.2214/AJR.18.20224>
- [5] A. J. London, Artificial Intelligence and Black-Box Medical Decisions: Accuracy versus Explainability, *Hastings Center Report* 49 (1) (2019) 15–21. doi:10.1002/hast.973.
- [6] A. Das, P. Rad, Opportunities and Challenges in Explainable Artificial Intelligence (XAI): A Survey, *Diabetes Care* 41 (2020) 1–24. arXiv:2006.11371.
URL <http://arxiv.org/abs/2006.11371>
- [7] P. P. Angelov, E. A. Soares, R. Jiang, N. I. Arnold, P. M. Atkinson, Explainable artificial intelligence: an analytical review, *Wiley Interdisciplinary Reviews: Data Mining and Knowledge Discovery* 11 (5) (2021) 1–13. doi:10.1002/widm.1424.
- [8] R. Miotto, F. Wang, S. Wang, X. Jiang, J. T. Dudley, Deep learning for healthcare: review, opportunities and challenges, *Briefings in Bioinformatics* 19 (6) (2017) 1236–1246. arXiv:<https://academic.oup.com/bib/article-pdf/19/6/1236/27119191/bbx044.pdf>, doi:10.1093/bib/bbx044.
URL <https://doi.org/10.1093/bib/bbx044>
- [9] A. S. Adamson, A. Smith, Machine Learning and Health Care Disparities in Dermatology, *JAMA Dermatology* 154 (11) (2018) 1247. doi:10.1001/jamadermatol.2018.2348.
URL <http://archderm.jamanetwork.com/article.aspx?doi=10.1001/jamadermatol.2018.2348>
- [10] M. Du, F. Yang, N. Zou, X. Hu, Fairness in deep learning: A computational perspective, *IEEE Intelligent Systems* 36 (4) (2021) 25–34. doi:10.1109/MIS.2020.3000681.

- [11] M. MacCarthy, An Examination of the Algorithmic Accountability Act of 2019, SSRN Electronic Journal (2020) 1–10doi:10.2139/ssrn.3615731.
- [12] Goodman Bryce, Flaxman Seth, European Union Regulations on Algorithmic Decision Making and a “Right to Explanation”, AI magazine 38 (3) (2017) 50–57.
- [13] R. Guidotti, A. Monreale, D. Pedreschi, F. Giannotti, Principles of Explainable Artificial Intelligence, Explainable AI Within the Digital Transformation and Cyber Physical Systems (2021) 9–31doi:10.1007/978-3-030-76409-8_2.
- [14] X.-H. Li, C. C. Cao, Y. Shi, W. Bai, H. Gao, L. Qiu, C. Wang, Y. Gao, S. Zhang, X. Xue, L. Chen, A Survey of Data-driven and Knowledge-aware eXplainable AI, IEEE Transactions on Knowledge and Data Engineering 34 (1) (2022) 29–49. doi:10.1109/TKDE.2020.2983930.
URL <https://ieeexplore.ieee.org/document/9050829/>
- [15] I. Tiddi, S. Schlobach, Knowledge graphs as tools for explainable machine learning: A survey, Artificial Intelligence 302 (2022) 103627. doi:<https://doi.org/10.1016/j.artint.2021.103627>.
URL <https://www.sciencedirect.com/science/article/pii/S0004370221001788>
- [16] G. Booch, F. Fabiano, L. Horesh, K. Kate, J. Lenchner, N. Linck, A. Loreggia, K. Murugesan, N. Mattei, F. Rossi, B. Srivastava, Thinking fast and slow in ai (2020). doi:10.48550/ARXIV.2010.06002.
URL <https://arxiv.org/abs/2010.06002>
- [17] D. N. Nicholson, C. S. Greene, Constructing knowledge graphs and their biomedical applications, Computational and Structural Biotechnology Journal 18 (2020) 1414–1428. doi:<https://doi.org/10.1016/j.csbj.2020.05.017>.
URL <https://www.sciencedirect.com/science/article/pii/S2001037020302804>
- [18] W. L. Wong, X. Su, X. Li, C. M. G. Cheung, R. Klein, C. Y. Cheng, T. Y. Wong, Global prevalence of age-related macular degeneration and disease burden projection for 2020 and 2040: A systematic review and meta-analysis, The Lancet Global Health 2 (2) (2014) e106–e116. doi:10.1016/S2214-109X(13)70145-1.
URL [http://dx.doi.org/10.1016/S2214-109X\(13\)70145-1](http://dx.doi.org/10.1016/S2214-109X(13)70145-1)
- [19] D. Śpiewak, Ł. Drzyzga, M. Dorecka, D. Wyględowska-Promieńska, Summary of the Therapeutic Options for Patients with Dry and Neovascular AMD, Journal of Clinical Medicine 13 (14) (2024). doi:10.3390/jcm13144227.
- [20] C. N. Thomas, D. A. Sim, W. H. Lee, N. Alfahad, A. D. Dick, A. K. Denniston, L. J. Hill, Emerging therapies and their delivery for treating age-related macular degeneration, British Journal of Pharmacology 179 (9) (2022) 1908–1937. doi:10.1111/bph.15459.

- [21] E. Y. Chew, Age-related Macular Degeneration: Nutrition, Genes and Deep Learning—The LXXVI Edward Jackson Memorial Lecture, *American Journal of Ophthalmology* 217 (2020) 335–347. doi: 10.1016/j.ajo.2020.05.042.
URL <https://doi.org/10.1016/j.ajo.2020.05.042>
- [22] X. Liu, L. Faes, A. U. Kale, S. K. Wagner, D. J. Fu, A. Bruynseels, T. Mahendiran, G. Moraes, M. Shamdas, C. Kern, J. R. Ledsam, M. K. Schmid, K. Balaskas, E. J. Topol, L. M. Bachmann, P. A. Keane, A. K. Denniston, A comparison of deep learning performance against health-care professionals in detecting diseases from medical imaging: a systematic review and meta-analysis, *The Lancet Digital Health* 1 (6) (2019) e271–e297. doi:10.1016/S2589-7500(19)30123-2.
URL [http://dx.doi.org/10.1016/S2589-7500\(19\)30123-2](http://dx.doi.org/10.1016/S2589-7500(19)30123-2)
- [23] L. Gherardini, V. R. Varma, K. Capała, R. Woods, J. Sousa, CACTUS: a Comprehensive Abstraction and Classification Tool for Uncovering Structures, *ACM Transactions on Intelligent Systems and Technology* (feb 2024). arXiv:2308.12031, doi:10.1145/3649459.
URL <https://dl.acm.org/doi/10.1145/3649459>
- [24] M. Garnelo, M. Shanahan, Reconciling deep learning with symbolic artificial intelligence: representing objects and relations, *Current Opinion in Behavioral Sciences* 29 (2019) 17–23, artificial Intelligence. doi:<https://doi.org/10.1016/j.cobeha.2018.12.010>.
URL <https://www.sciencedirect.com/science/article/pii/S2352154618301943>
- [25] N. Salimiaghdam, M. Riazi-Esfahani, P. S. Fukuhara, K. Schneider, M. C. Kenney, Age-related Macular Degeneration (AMD): A Review on its Epidemiology and Risk Factors, *The Open Ophthalmology Journal* 13 (1) (2020) 90–99. doi:10.2174/1874364101913010090.
- [26] T. D. Keenan, S. Vitale, E. Agrón, A. Domalpally, A. N. Antoszyk, M. J. Elman, T. E. Clemons, E. Y. Chew, Visual Acuity Outcomes after Anti-Vascular Endothelial Growth Factor Treatment for Neovascular Age-Related Macular Degeneration, *Ophthalmology Retina* 4 (1) (2020) 3–12. doi: 10.1016/j.oret.2019.06.001.
URL <https://linkinghub.elsevier.com/retrieve/pii/S2468653019300739>
- [27] C.-J. Chiu, R. Klein, R. C. Milton, G. Gensler, A. Taylor, Does eating particular diets alter the risk of age-related macular degeneration in users of the age-related eye disease study supplements?, *British Journal of Ophthalmology* 93 (9) (2009) 1241–1246. arXiv:<https://bjo.bmj.com/content/93/9/1241.full.pdf>, doi:10.1136/bjo.2008.143412.
URL <https://bjo.bmj.com/content/93/9/1241>
- [28] Q. Yan, D. E. Weeks, H. Xin, A. Swaroop, E. Y. Chew, H. Huang, Y. Ding, W. Chen, Deep-learning-based prediction of late age-related macular degeneration progression, *Nature Machine Intelligence* 2 (2) (2020) 141–150. doi:10.1038/s42256-020-0154-9.
URL <http://dx.doi.org/10.1038/s42256-020-0154-9>

- [29] P. M. Burlina, N. Joshi, M. Pekala, K. D. Pacheco, D. E. Freund, N. M. Bressler, Automated grading of age-related macular degeneration from color fundus images using deep convolutional neural networks, *JAMA Ophthalmology* 135 (11) (2017) 1170–1176. doi:10.1001/jamaophthalmol.2017.3782.
- [30] P. M. Burlina, N. Joshi, K. D. Pacheco, D. E. Freund, J. Kong, N. M. Bressler, Use of Deep Learning for Detailed Severity Characterization and Estimation of 5-Year Risk among Patients with Age-Related Macular Degeneration, *JAMA Ophthalmology* 136 (12) (2018) 1359–1366. doi:10.1001/jamaophthalmol.2018.4118.
- [31] U. Schmidt-Erfurth, A. Sadeghipour, B. S. Gerendas, S. M. Waldstein, H. Bogunović, Artificial intelligence in retina, *Progress in Retinal and Eye Research* 67 (May) (2018) 1–29. doi:10.1016/j.preteyeres.2018.07.004.
URL <https://doi.org/10.1016/j.preteyeres.2018.07.004>
- [32] M. Michl, M. Fabianska, P. Seeböck, A. Sadeghipour, B. H. Najeeb, H. Bogunovic, U. M. Schmidt-Erfurth, B. S. Gerendas, Automated quantification of macular fluid in retinal diseases and their response to anti-VEGF therapy, *British Journal of Ophthalmology* (2020) 1–8doi: 10.1136/bjophthalmol-2020-317416.
- [33] T. Perepelkina, A. B. Fulton, Artificial Intelligence (AI) Applications for Age-Related Macular Degeneration (AMD) and Other Retinal Dystrophies, *Seminars in Ophthalmology* 36 (4) (2021) 304–309. doi:10.1080/08820538.2021.1896756.
URL <https://doi.org/10.1080/08820538.2021.1896756>
- [34] D. S. W. Ting, C. Y. L. Cheung, G. Lim, G. S. W. Tan, N. D. Quang, A. Gan, H. Hamzah, R. Garcia-Franco, I. Y. S. Yeo, S. Y. Lee, E. Y. M. Wong, C. Sabanayagam, M. Baskaran, F. Ibrahim, N. C. Tan, E. A. Finkelstein, E. L. Lamoureux, I. Y. Wong, N. M. Bressler, S. Sivaprasad, R. Varma, J. B. Jonas, M. G. He, C. Y. Cheng, G. C. M. Cheung, T. Aung, W. Hsu, M. L. Lee, T. Y. Wong, Development and validation of a deep learning system for diabetic retinopathy and related eye diseases using retinal images from multiethnic populations with diabetes, *JAMA - Journal of the American Medical Association* 318 (22) (2017) 2211–2223. doi:10.1001/jama.2017.18152.
- [35] H. Bogunović, S. M. Waldstein, T. Schlegl, G. Langs, A. Sadeghipour, X. Liu, B. S. Gerendas, A. Osborne, U. Schmidt-Erfurth, Prediction of Anti-VEGF Treatment Requirements in Neovascular AMD Using a Machine Learning Approach, *Investigative Ophthalmology and Visual Science* 58 (7) (2017) 3240–3248. doi:10.1167/iovs.16-21053.
- [36] C. Delcourt, J. F. Korobelnik, G. H. Buitendijk, P. J. Foster, C. J. Hammond, S. Piermarocchi, T. Peto, N. Jansonius, A. Mirshahi, R. E. Hogg, L. Bretillon, F. Topouzis, G. Deak, J. Grauslund, R. Broe, E. H. Souied, C. Creuzot-Garcher, J. Sahel, V. Daïen, T. Lehtimäki, H. W. Hense,

- E. Prokofyeva, K. Oexle, J. S. Rahi, P. M. Cumberland, S. Schmitz-Valckenberg, S. Fauser, G. Bertelsen, C. Hoyng, A. Bergen, R. Silva, S. Wolf, A. Lotery, U. Chakravarthy, A. Fletcher, C. C. Klaver, Ophthalmic epidemiology in Europe: the “European Eye Epidemiology” (E3) consortium, *European Journal of Epidemiology* 31 (2) (2016) 197–210. doi:10.1007/s10654-015-0098-2.
- [37] T. P. Peixoto, The graph-tool python library, figshare (2014). doi:10.6084/m9.figshare.1164194.
- [38] D. F. Gleich, Pagerank beyond the web, *SIAM Review* 57 (3) (2015) 321–363. arXiv:<https://doi.org/10.1137/140976649>, doi:10.1137/140976649.
URL <https://doi.org/10.1137/140976649>
- [39] I. Nouretdinov, S. G. Costafreda, A. Gammerman, A. Chervonenkis, V. Vovk, V. Vapnik, C. H. Fu, Machine learning classification with confidence: Application of transductive conformal predictors to mri-based diagnostic and prognostic markers in depression, *NeuroImage* 56 (2) (2011) 809–813, multivariate Decoding and Brain Reading. doi:<https://doi.org/10.1016/j.neuroimage.2010.05.023>.
URL <https://www.sciencedirect.com/science/article/pii/S105381191000755X>
- [40] T. A. Johansen, On tikhonov regularization, bias and variance in nonlinear system identification, *Automatica* 33 (3) (1997) 441–446. doi:[https://doi.org/10.1016/S0005-1098\(96\)00168-9](https://doi.org/10.1016/S0005-1098(96)00168-9).
- [41] M. P. LaValley, Logistic regression, *Circulation* 117 (18) (2008) 2395–2399. doi:10.1161/CIRCULATIONAHA.106.682658.
- [42] C. Cortes, V. Vapnik, Support-vector networks, *Machine Learning* 20 (3) (1995) 273–297. doi:10.1007/BF00994018.
- [43] S. ichi Amari, Backpropagation and stochastic gradient descent method, *Neurocomputing* 5 (4) (1993) 185–196. doi:[https://doi.org/10.1016/0925-2312\(93\)90006-0](https://doi.org/10.1016/0925-2312(93)90006-0).
- [44] L. Breiman, Random Forests, *Machine Learning* 45 (2001) 5–32. doi:<https://doi.org/10.1023/A:1010933404324>.
- [45] T. Chen, C. Guestrin, Xgboost: A scalable tree boosting system, in: *Proceedings of the 22nd ACM SIGKDD International Conference on Knowledge Discovery and Data Mining, KDD ’16*, Association for Computing Machinery, New York, NY, USA, 2016, p. 785–794. doi:10.1145/2939672.2939785.
URL <https://doi.org/10.1145/2939672.2939785>
- [46] G. Van Rossum, F. L. Drake, *Python 3 Reference Manual*, CreateSpace, Scotts Valley, CA, 2009.
- [47] F. Pedregosa, G. Varoquaux, A. Gramfort, V. Michel, B. Thirion, O. Grisel, M. Blondel, P. Prettenhofer, R. Weiss, V. Dubourg, J. Vanderplas, A. Passos, D. Cournapeau, M. Brucher, M. Perrot, E. Duchesnay, Scikit-learn: Machine learning in Python, *Journal of Machine Learning Research* 12 (2011) 2825–2830.

- [48] X. Ying, An Overview of Overfitting and its Solutions, Journal of Physics: Conference Series 1168 (2) (2019). doi:10.1088/1742-6596/1168/2/022022.
- [49] H. White, Parametric statistical estimation with artificial neural networks: A condensed discussion", booktitle="from statistics to neural networks, Springer Berlin Heidelberg, Berlin, Heidelberg, 1994, pp. 127–146.
- [50] T. Hellström, A Random Walk through the Stock Market, Doctoral dissertation (1998).
URL <http://e-m-h.org/Hell98.pdf>

Supplementary

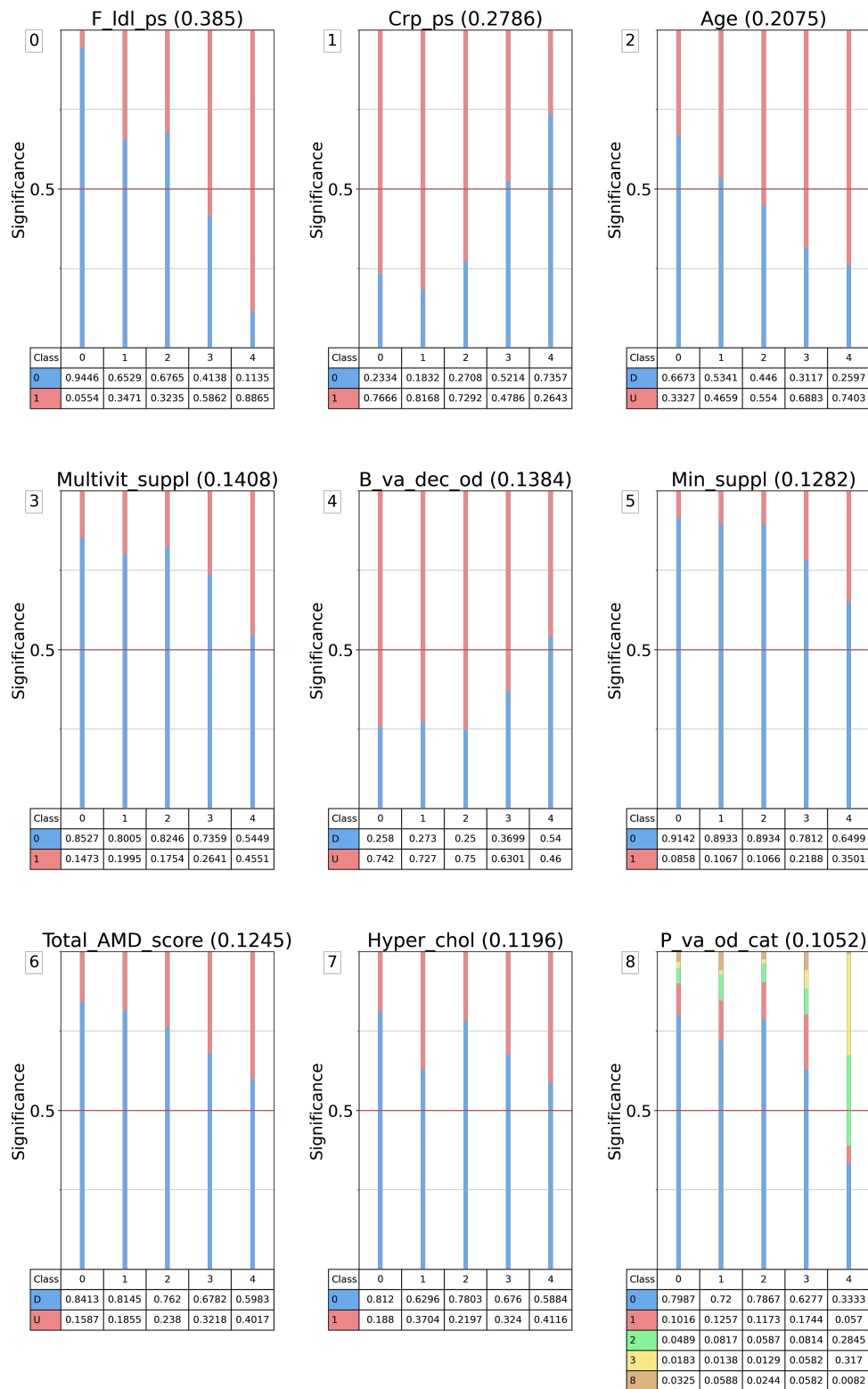


Figure 5: Feature ranks computed by CACTUS through the *Degree* centrality on the knowledge graphs. They are sorted from the highest (upper left) to the lowest (lower right), as indicated in the title of each plot between parentheses.

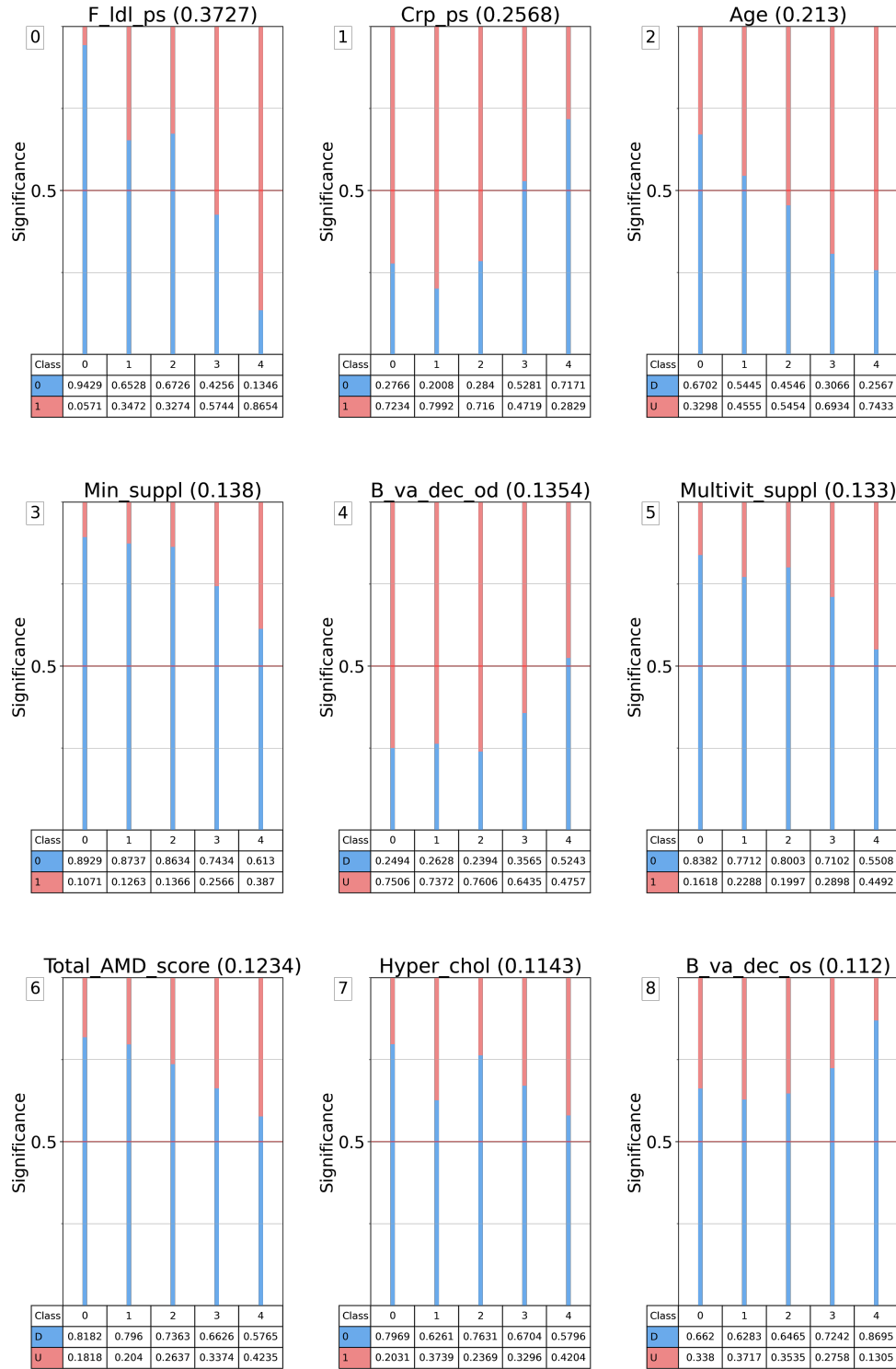


Figure 6: The ranks of the features computed by CACTUS through the *PageRank* centrality on the knowledge graphs. They are sorted from the highest (upper left) to the lowest (lower right), as indicated in the title of each plot between parentheses.

CDG		CPR		CPB	
Marker	Rank	Marker	Rank	Marker	Rank
F_ldl_ps	.3963	F_ldl_ps	.3845	F_ldl_ps	.3748

Crp_ps	.2826	Crp_ps	.2609	Crp_ps	.266
Age	.2024	Age	.2087	Age	.2008
Multivit_suppl	.1451	B_va_dec_od	.1415	Acar	.1767
B_va_dec_od	.143	Multivit_suppl	.1348	Crypto	.149
Acar	.1364	Min_suppl	.1344	Flavoproteins	.149
Min_suppl	.1254	Hyper_chol	.1198	Lycop	.149
Hyper_chol	.1241	Acar	.1178	Lut_zea	.1485
Total_AMD_score	.1156	Total_AMD_score	.1163	Multivit_suppl	.145
P_va_od_cat	.1024	Trombo_inh	.1103	B_va_dec_od	.1363
Trombo_inh	.1011	B_va_dec_os	.1057	Min_suppl	.1266
ARMS2_rs3750846	.0953	P_va_od_cat	.1002	Hyper_chol	.1224
B_va_dec_os	.0949	Nsaid	.0989	Pufa_omg6	.1224
Ses	.0921	Ses	.098	Total_AMD_score	.1116
P_va_os_cat	.0898	B_va_os_cat	.095	B9	.1049
Nsaid	.0895	B_va_od_cat	.0927	B3	.1043
CFH_rs10922109	.0893	P_va_os_cat	.0882	Epa_dha	.1036
B_va_os_cat	.0877	Outside	.0844	B1	.1035
Outside	.0867	ARMS2_rs3750846	.0843	B2	.1035
Complement_score	.0865	Complement_score	.0804	Bcar	.1026
B_va_od_cat	.0856	Risk_ARMS2	.0771	Pufa_omg3	.1026
Risk_ARMS2	.0805	Vitamind_ps	.0752	Trombo_inh	.1016
Vitamind_ps	.077	Fishoil_suppl	.0702	B_carotene	.1012
CFH_rs570618	.0764	Omeg3_suppl	.0702	P_va_od_cat	.098
Fishoil_suppl	.0752	Iris_color	.0672	B_va_dec_os	.0952
Omeg3_suppl	.0752	CFH_rs10922109	.0662	ARMS2_rs3750846	.0911
Pufa_omg6	.074	CFH_rs570618	.063	Outside	.0874
Iris_color	.0675	Pufa_omg6	.0609	CFH_rs10922109	.0865
Tei	.0632	Refr_cyl_os	.0596	Dairy_freq	.0862
Vitd	.0569	F_hdl_ps	.0595	Egg_freq	.0862
Vitc	.0551	Hypertension	.0595	Legume_freq	.0862
Vitamind	.0544	Refr_cyl_od	.0585	Vegetable_freq	.0862
Hypertension	.0534	F_choles_ps	.0565	White_meat_freq	.0862
Cessation_a	.053	Vitamind	.0561	P_va_os_cat	.0854
Refr_cyl_od	.0522	Anti_vegf_any	.0551	B_va_os_cat	.0843
Pressure_sys	.0509	Pressure_sys	.0543	Nsaid	.0839
P_va_dec_os	.0491	Cessation_a	.0534	Fish_freq	.0834
Refr_cyl_os	.0488	Refr_sph_od	.0534	Meat_freq	.0834

Anti_vegf_any	.0486	F_trigly_ps	.053	Red_meat_freq	.0834
Smoke_ever	.0475	Cylinder_sign_os	.0523	Complement_score	.0827
Alcohol_ever	.0473	Tei	.052	B_va_od_cat	.0822
C2_rs114254831	.046	C2_rs114254831	.0513	Risk_ARMS2	.0772
F_hdl_ps	.0455	P_va_dec_os	.0513	CFH_rs570618	.0741
Refr_axis_od	.0454	Alcohol_ever	.0507	Vitamind_ps	.0718
Refr_sph_od	.0448	Cylinder_sign_od	.0505	Lung_disease	.0692
Cylinder_sign_os	.0439	Vitd	.0503	Tot_prot	.0684
F_choles_ps	.043	Vitc	.0481	Iris_color	.066
Height	.0423	Lens_od	.048	Ses	.0653
Lens_od	.0423	Anti_diab	.0477	Hypertension	.0599
Lipid_score	.0418	Lens_os	.0477	Tei	.0586
Cylinder_sign_od	.0417	Physical_act	.0466	Cessation_a	.0566
C3_rs2230199	.0416	Smoke_ever	.0462	Zeaxanthin	.0538
Anti_hyp	.0412	F_glucose_ps	.0451	Smoke_ever	.0529
Refr_axis_os	.04	P_va_dec_od	.0442	Cylinder_sign_os	.0518
NPLOC4_rs6565597	.0399	F_trigly	.044	Lutein	.0514
F_trigly_ps	.0397	Cardiovasc	.0433	Tot_carb	.0512
ECM_Score	.0396	C3_rs2230199	.0429	Refr_cyl_od	.0508
Lens_os	.0393	NPLOC4_rs6565597	.0419	Pressure_sys	.05
CFH_rs61818925	.0391	Pufa	.0409	Cylinder_sign_od	.0494
TRPM3_rs71507014	.0389	Anti_vegf_od	.0396	Anti_vegf_any	.0492
Anti_diab	.0377	Refr_axis_od	.0385	Vitc	.0487
P_va_dec_od	.0368	Anti_glauc	.038	F_hdl_ps	.0486
Gfr	.0367	Anti_hyp	.038	Refr_cyl_os	.0475
LIPC_rs2043085	.0367	Mufa_sfa	.0379	Alcohol_ever	.0465
F_glucose_ps	.0362	TRPM3_rs71507014	.0375	F_choles_ps	.0463
Refr_sph_os	.0356	Gfr	.0372	Nf_glucose	.046
F_trigly	.035	Height	.0362	Refr_sph_od	.046
Cardiovasc	.0346	Olive_qtt	.0362	Vitamind	.0458
Anti_vegf_od	.0345	Crp	.0361	C2_rs114254831	.0456
F_hdl	.0339	Lipid_score	.0361	Anti_hyp	.0436
CNN2_rs67538026	.0334	A_length_od	.0359	Vitd	.0435
Crp	.0323	Sfa	.0353	Refr_axis_od	.0434
Physical_act	.0323	Refr_sph_os	.0351	Anti_diab	.0432
Alat	.032	CNN2_rs67538026	.0348	CNN2_rs67538026	.0425
Mufa_sfa	.0318	Vegetable_qtt	.0347	F_trigly_ps	.0425

C2_rs943080	.0315	ECM_Score	.0336	F_glucose_ps	.0422
Pufa	.0303	Red_meat_qtt	.0327	B12	.0418
Anti_glauc	.0298	Refr_axis_os	.0321	B6	.0412
P_va_letters_od	.0293	P_va_letters_od	.0319	Crp	.0409
Tot_carb	.0285	Beer	.0306	Vite	.0409
B_va_od	.0278	Alzheimer	.0305	Lens_od	.0401
Olive_qtt	.0274	Gamma_gt	.03	P_va_dec_os	.04
Red_meat_qtt	.0274	LIPC_rs2043085	.03	Refr_axis_os	.0399
SLC16A8_rs8135665	.0268	Alat	.0299	Height	.0397
Anti_vegf_os	.0265	Anti_vegf_os	.0298	C3_rs2230199	.0395
A_length_od	.0258	Nuts_qtt	.029	Lipid_score	.0394
COL8A1_rs55975637	.0256	F_hdl	.0285	CFH_rs61818925	.0386
Alcohol	.0254	CFH_rs61818925	.0281	Fishoil_suppl	.0384
Vegetable_qtt	.0252	C2_rs943080	.0278	Omeg3_suppl	.0384
Alzheimer	.0251	B_va_od	.0265	NPLOC4_rs6565597	.0381
Beer	.0243	Wine	.0261	Zinc_food	.0377
CETP_rs5817082	.0241	SLC16A8_rs8135665	.0257	F_trigly	.0375
Sfa	.0241	Asat	.0254	Lens_os	.0371
Bmi	.024	Egg_qtt	.0252	ECM_Score	.037
Urea	.0239	COL8A1_rs55975637	.0247	Refr_sph_os	.037
Meat_freq	.0235	CETP_rs5817082	.0244	Anti_vegf_od	.0364
Red_meat_freq	.0235	Lipid_low	.0237	LIPC_rs2043085	.0362
Vite	.0233	Cessation_y	.0234	Cardiovasc	.0358
PILRB_rs7803454	.0229	Alcohol	.0231	P_va_letters_od	.035
B6	.0226	A_length_os	.0228	Alat	.0342
Cessation_y	.0225	Tot_carb	.0227	Gfr	.0339
Pressure_od	.0225	Bmi	.0214	TRPM3_rs71507014	.0327
Wine	.0222	Oily_qtt	.0207	F_hdl	.0316
CETP_rs17231506	.0218	Dairy_qtt	.0206	Urea	.0315
ABCA1_rs2740488	.0211	Diabetes	.0202	C2_rs943080	.0312
B_va_os	.0211	Zeaxanthin	.0202	Anti_glauc	.0293
Dairy_freq	.0207	B_va_os	.0201	Physical_act	.0293
Egg_freq	.0207	Liquor	.0201	Wine	.0293
Legume_freq	.0207	MMP9_rs142450006	.02	B_va_od	.0291
Vegetable_freq	.0207	PILRB_rs7803454	.0199	Anti_vegf_os	.0279
Nuts_qtt	.0202	Pmeat_qtt	.0199	F_ldl	.0279
Oily_qtt	.0196	LIPC_rs2070895	.0197	Pressure_od	.0272

RAD51B_rs61985136	.0195	SYN3_rs5754227	.0193	Bmi	.0264
Zeaxanthin	.0193	COL4A3_rs11884770	.0192	Pack_years	.0263
Egg_qtt	.019	Meat_qtt	.0188	P_va_letters_os	.0258
ARHGAP21_rs12357257	.0189	Urea	.0184	Pmeat_qtt	.0257
Liquor	.0189	B6	.0183	Red_meat_qtt	.0257
LIPC_rs2070895	.0182	Vite	.0183	Alzheimer	.0256
Lipid_low	.0182	Meat_freq	.018	A_length_od	.0253
F_choles	.018	Red_meat_freq	.018	Alcohol	.0252
COL4A3_rs11884770	.0177	RAD51B_rs61985136	.0178	P_va_dec_od	.0252
Gamma_gt	.0175	APOE_rs429358	.0176	A_length_os	.0245
Pmeat_qtt	.0175	Legume_qtt	.0176	CETP_rs5817082	.0243
APOE_rs73036519	.0171	ABCA1_rs2740488	.0175	SLC16A8_rs8135665	.0242
TMEM97_rs11080055	.0166	Fish_qtt	.0174	Pufa	.024
Legume_qtt	.0163	Pressure_od	.0171	COL8A1_rs55975637	.0235
Fish_qtt	.016	TGFBR1_rs1626340	.0166	Liquor	.023
CFI_rs10033900	.0159	Weight	.0163	Beer	.0228
Smoke_start	.0159	ARHGAP21_rs12357257	.0158	Mufa_sfa	.0215
TNFRSF10A_rs79037040	.0159	Mufa	.0155	Cessation_y	.0212
APOE_rs429358	.0158	Dairy_freq	.0153	Sfa	.0206
Dairy_qtt	.0156	Egg_freq	.0153	PILRB_rs7803454	.0205
MIR6130_rs10781182	.0155	Legume_freq	.0153	Meat_qtt	.02
W_circ	.0155	Vegetable_freq	.0153	Vegetable_qtt	.02
Asat	.0153	F_idl	.0146	ABCA1_rs2740488	.0199
Diabetes	.015	H_circ	.0146	CETP_rs17231506	.0199
ADAMTS9_rs62247658	.0149	P_va_letters_os	.0145	LIPC_rs2070895	.0199
RAD51B_rs2842339	.0149	C20orf85_rs201459901	.0144	B_va_os	.0197
SYN3_rs5754227	.0148	CETP_rs17231506	.0143	RAD51B_rs61985136	.0196
Pressure_os	.0146	APOE_rs73036519	.0141	Lipid_low	.0191
A_length_os	.0141	Cigarette	.0141	White_qtt	.0191
Meat_qtt	.0141	RAD51B_rs2842339	.0138	ARHGAP21_rs12357257	.0181
B3GALT_rs9564692	.0138	TMEM97_rs11080055	.0138	F_choles	.0181
Tot_prot	.0134	B3GALT_rs9564692	.0134	Olive_qtt	.018
KMT2E_rs1142	.0129	Smoke_start	.0133	COL4A3_rs11884770	.0176
Lung_disease	.0129	MIR6130_rs10781182	.0127	Smoke_start	.0176
MMP9_rs142450006	.0127	Cortico	.0124	Cereal_qtt	.0173
F_idl	.0126	Pressure_os	.0123	APOE_rs73036519	.0164
B12	.0125	Lutein	.0122	Pressure_os	.0164

Weight	.0121	TNFRSF10A_rs79037040	.0122	MMP9_rs142450006	.0162
Lutein	.012	C3_rs12019136	.012	SYN3_rs5754227	.0162
TGFBR1_rs1626340	.0119	ADAMTS9_rs62247658	.0119	TNFRSF10A_rs79037040	.0155
Cigarette	.0117	F_choles	.0119	Fruit_qtt	.0153
Zinc_food	.0117	CFI_rs10033900	.0118	TMEM97_rs11080055	.0152
Fish_freq	.0116	CTRB2_rs72802342	.0115	Diabetes	.0151
C20orf85_rs201459901	.0113	C2_rs429608	.011	White_meat_qtt	.0151
P_va_letters_os	.0113	Suppl_amd	.011	APOE_rs429358	.015
F_glucose	.0111	W_circ	.0105	CFI_rs10033900	.015
Cortico	.0107	CFH_rs187328863	.0104	MIR6130_rs10781182	.0149
H_circ	.0107	RDH5_rs3138141	.0104	Mufa	.0149
C3_rs12019136	.0102	C3_rs147859257	.0099	Nuts_qtt	.0147
Suppl_amd	.0094	Fish_freq	.0099	RAD51B_rs2842339	.0144
CTRB2_rs72802342	.0092	KMT2E_rs1142	.0099	ADAMTS9_rs62247658	.0143
C3_rs147859257	.0091	Pressure_dias	.0098	Gamma_gt	.0142
Pack_years	.0091	Pack_years	.0096	Weight	.0138
C9_rs62358361	.0089	C9_rs62358361	.0095	Asat	.0137
B2	.0087	B12	.0094	TGFBR1_rs1626340	.0131
CFH_rs187328863	.0085	F_glucose	.0094	C20orf85_rs201459901	.0129
RDH5_rs3138141	.0085	Lung_disease	.0093	B3GALT_rs9564692	.0127
Fruit_qtt	.0083	Fruit_qtt	.0085	Cigarette	.0127
Mufa	.0082	Tot_prot	.0085	W_circ	.0126
B1	.0078	Pipe	.0083	KMT2E_rs1142	.0123
C2_rs429608	.0073	White_meat_qtt	.0082	C3_rs12019136	.0115
Pressure_dias	.007	Zinc_food	.0079	Fish_qtt	.0115
White_meat_qtt	.0067	B2	.0077	Egg_qtt	.0111
Pufa_omg3	.0066	B1	.0065	Suppl_amd	.0108
Bcar	.0063	COL8A1_rs140647181	.0064	F_glucose	.0107
COL8A1_rs140647181	.0062	Nf_glucose	.0058	CTRB2_rs72802342	.0105
Lycop	.006	CFH_rs191281603	.0055	H_circ	.01
White_meat_freq	.006	Lycop	.0053	Legume_qtt	.0095
Pipe	.0059	Pufa_omg3	.0053	Cortico	.0092
Nf_glucose	.0058	Bcar	.0051	C2_rs429608	.0083
CFH_rs191281603	.0053	C2_rs144629244	.0045	C9_rs62358361	.0079
Epa_dha	.0046	White_meat_freq	.0045	RDH5_rs3138141	.0079
C2_rs144629244	.0045	Cereal_qtt	.0043	CFH_rs187328863	.0076
CFH_rs35292876	.0041	ACAD10_rs61941274	.004	C3_rs147859257	.0075

ACAD10_rs61941274	.0038	C2_rs181705462	.004	Pressure_dias	.007
Cereal_qtt	.0036	White_qtt	.0037	COL8A1_rs140647181	.005
C2_rs181705462	.0035	CFH_rs35292876	.0036	CFH_rs121913059	.0041
White_qtt	.0035	Epa_dha	.003	CFH_rs148553336	.0039
B_carotene	.0034	CFI_rs141853578	.0028	CFH_rs191281603	.0037
Crypto	.0032	Crypto	.0027	C2_rs181705462	.0033
Flavoproteins	.0032	Flavoproteins	.0027	ACAD10_rs61941274	.0032
CFI_rs141853578	.0029	B_carotene	.0023	PRLR_SPEF2_rs114092250	.0031
B9	.0026	B9	.0022	C2_rs144629244	.003
Lut_zea	.0025	CFH_rs148553336	.0021	Dairy_qtt	.0029
B3	.0017	Lut_zea	.0015	Pipe	.0029
CFH_rs148553336	.0016	PRLR_SPEF2_rs114092250	.0014	CFH_rs35292876	.002
PRLR_SPEF2_rs114092250	.0012	B3	.0013	CFI_rs141853578	.0015
CFH_rs121913059	.0008	CFH_rs121913059	.0006	Oily_qtt	.0011

Table 4: Ranking of each feature in the EYE-RISK dataset performed by the three CACTUS classification modalities: Degree (CDG), PageRank (CPR), and Probabilistic (CPB).

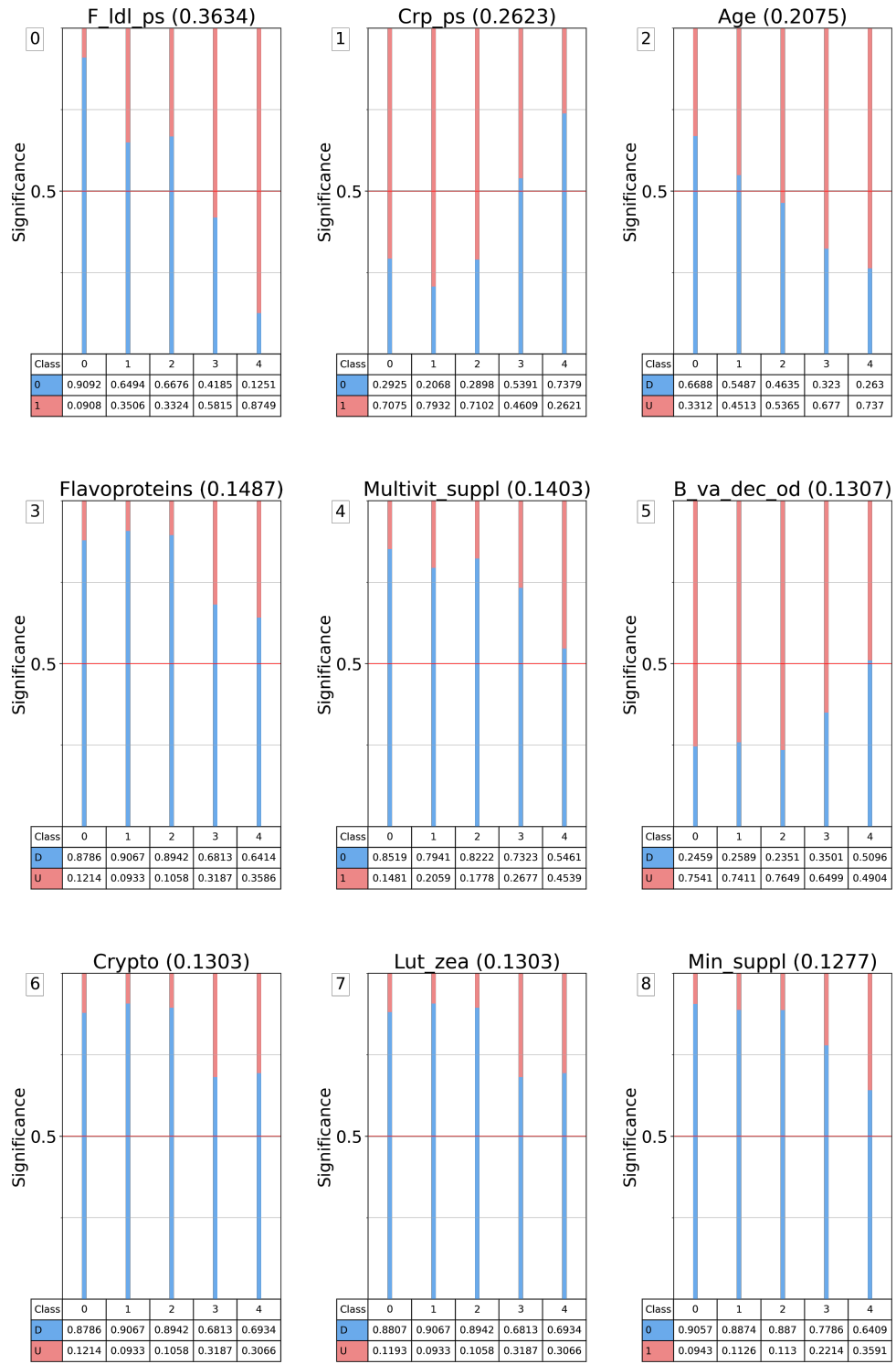


Figure 7: Feature ranks computed by CACTUS through the *Probabilistic* significance metric. They are sorted from the highest (upper left) to the lowest (lower right), as indicated in the title of each plot between parentheses. The scores do not sum up to 1 because of missing values.